Available online at www.sciencedirect.com
SCIENCE DIRECT®
ELSEVIER
Journal of Contaminant Hydrology 62–63 (2003) 613–636
JOURNAL OF Contaminant Hydrology
www.elsevier.com/locate/jconhyd

Testing and parameterizing a conceptual solute transport model in saturated fractured tuff using sorbing and nonsorbing tracers in cross-hole tracer tests

Paul W. Reimus[a,*], Marc J. Haga[a], Andrew I. Adams[a], Timothy J. Callahan[b], H.J. Turin[a], Dale A. Counce[c]

[a] *Environmental Science and Waste Technology Division, Los Alamos National Laboratory, P.O. Box 1663, MS J534, Los Alamos, NM 87545, USA*
[b] *Department of Geology and Environmental Sciences, College of Charleston, 66 George Street, Charleston, SC 29424, USA*
[c] *Earth and Environmental Sciences Division, Los Alamos National Laboratory, Los Alamos, NM 87545, USA*

Abstract

Two cross-hole tracer tests involving the simultaneous injection of two nonsorbing solute tracers with different diffusion coefficients (bromide and pentafluorobenzoate) and one weakly sorbing solute tracer (lithium ion) were conducted in two different intervals at the C-wells complex near the site of a potential high-level nuclear waste repository at Yucca Mountain, NV. The tests were conducted to (1) test a conceptual radionuclide transport model for saturated, fractured tuffs near Yucca Mountain and (2) obtain transport parameter estimates for predictive modeling of radionuclide transport. The differences between the responses of the two nonsorbing tracers and the sorbing tracer (when normalized to injection masses) were consistent with a dual-porosity transport system in which matrix diffusion was occurring. The concentration attenuation of the sorbing tracer relative to the nonsorbing tracers suggested that diffusion occurred primarily into matrix pores, not simply into stagnant water within the fractures. The K_d values deduced from the lithium responses were generally larger than K_d values measured in laboratory batch sorption tests using crushed C-wells cores. This result supports the use of laboratory-derived K_d values for predicting sorbing species transport at the site, as the laboratory K_d values would result in underprediction of sorption and hence conservative transport predictions. The tracer tests also provided estimates of effective flow porosity and longitudinal dispersivity at the site. The tests

* Corresponding author. Tel.: +1-505-665-2537; fax: +1-505-665-4955.
E-mail address: preimus@lanl.gov (P.W. Reimus).

doi:10.1016/S0169-7722(02)00185-7

clearly demonstrated the advantages of using multiple tracers of different physical and chemical characteristics to distinguish between alternative conceptual transport models and to obtain transport parameter estimates that are better constrained than can be obtained using only a single tracer or using multiple nonsorbing tracers without a sorbing tracer.

Keywords: Tracers; Sorbing tracer(s); Matrix diffusion; Ion exchange; Multi-species; RELAP

1. Introduction

To support characterization of the saturated zone near Yucca Mountain, NV (Eddebbarh et al., 2003, this issue), a number of hydraulic and tracer tests were conducted at a three-well complex known as the C-wells (UE-25c#1, UE-25c#2, and UE-25c#3), located approximately 2 km southeast of the potential repository footprint. Fig. 1 shows the location and surface layout of the C-wells. The C-wells are 30.4–76.6 m apart at the land surface (Fig. 1), but they deviate substantially at depth.

The C-wells were completed to a depth of 914 m below land surface in easterly dipping Miocene tuffaceous rocks, which have been offset by high-angle, northerly and northwesterly trending faults. These rocks are pervaded by tectonic and cooling fractures that predominantly strike northward and dip westward at high angles (Geldon, 1996). The tuffs consist of nonwelded to densely welded ash-flow material with intervals of ash-fall tuff and volcaniclastic rocks. The geology below the water table at the C-wells is depicted in Fig. 2, along with fracture densities and estimated average matrix porosities in each unit (Geldon, 1993). In the C-wells, depths to water range from 400 to 402 m.

A consistent observation in all hydrogeologic units below the water table at the C-wells is that bulk permeabilities (determined from aquifer tests) exceed matrix permeabilities (determined from laboratory core measurements) by 2 to 6 orders of magnitude (Geldon, 1996, 1993). Flow logs in the C-wells indicate that most flow in the tuffs is from discrete fracture zones (triangles in Fig. 2). Although flow in the Miocene tuffs occurs predominantly in fractures, most of the water in the rocks is stored in the pores of the matrix. Matrix porosities in the C-wells range from about 0.10 to 0.35. Radionuclide and tracer transport in fractures, therefore, could be attenuated by diffusive mass transfer between the fractures and the rock matrix (matrix diffusion). Matrix diffusion in fractured systems has been discussed and modeled at length by Neretnieks (1980), Grisak and Pickens (1980), Tang et al. (1981), Maloszewski and Zuber (1984, 1985), and Moench (1995). A system exhibiting fracture and matrix flow frequently is called a "dual-porosity, dual-permeability" system. When the matrix permeability is small compared to the fracture permeability (e.g., smaller by a factor of 100 or more), the matrix permeability can be assumed negligible in transport calculations, and the system is then often referred to as simply a "dual-porosity" system. It has been suggested that the saturated zone in the Yucca Mountain vicinity should behave as a dual-porosity system (Robinson, 1994).

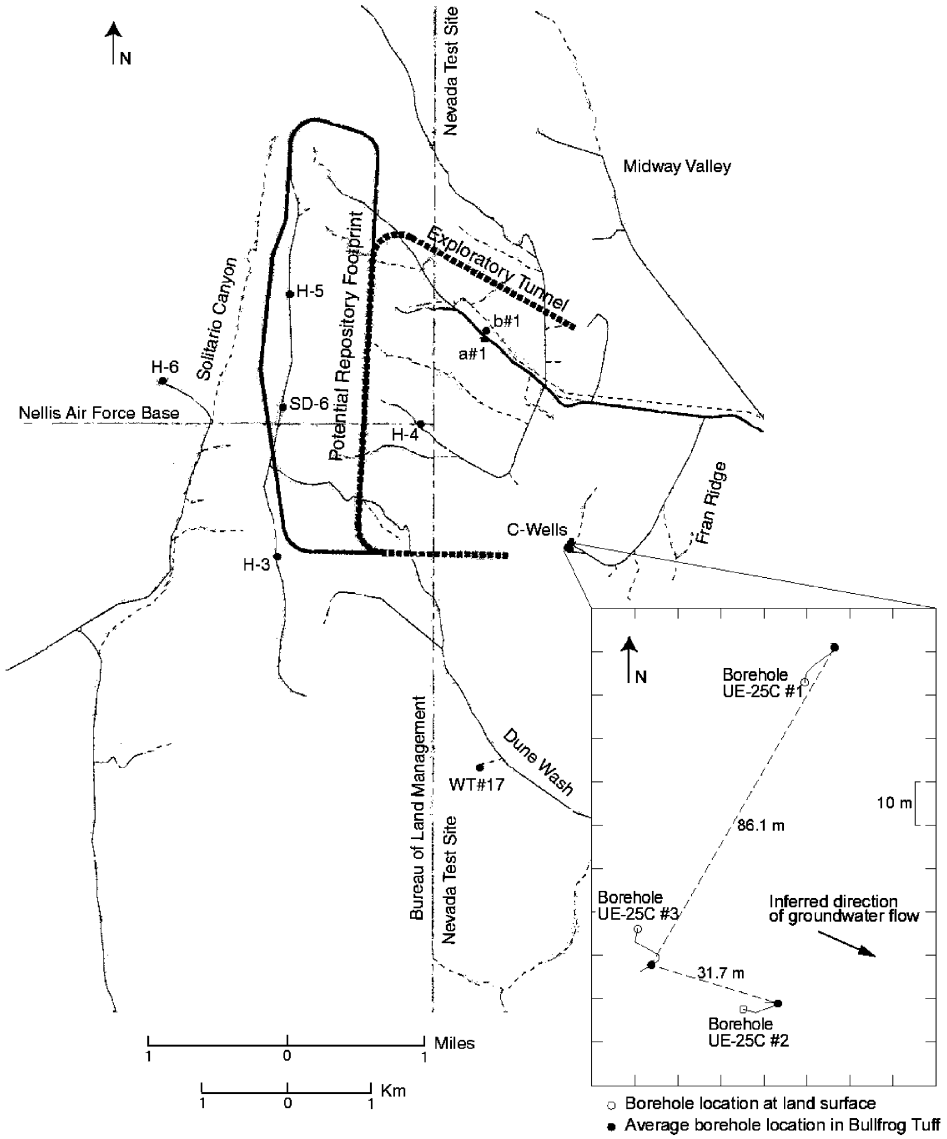

Fig. 1. Location and layout of the C-wells complex relative to potential repository footprint, exploratory tunnel, and selected wells in the vicinity of Yucca Mountain. Solid lines are improved surface roads; dashed lines are unimproved roads.

In 1996 and 1997, hydraulic and tracer tests were conducted in the lower part of the Bullfrog Tuff in the C-wells (packer locations shown in Fig. 2). A second round of hydraulic and tracer tests was conducted in the Prow Pass Tuff in 1998–1999 (packer

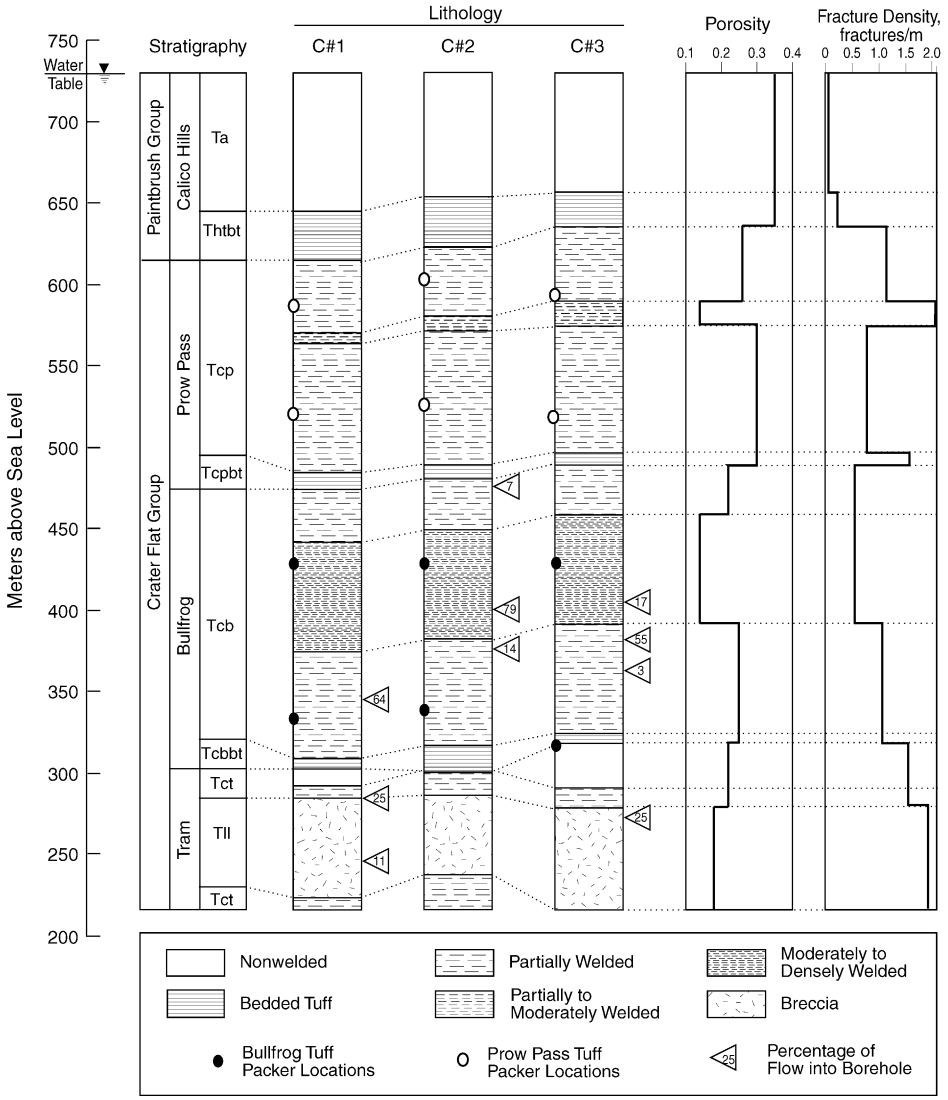

Fig. 2. Stratigraphy, lithology, matrix porosity, fracture density, and inflow (from open-hole flow surveys at the C-wells). Packer locations indicate intervals in which tracer tests described in this paper were conducted. Information derived from Geldon (1993).

locations also shown in Fig. 2). This paper presents the results and interpretation of two cross-hole tracer tests between wells C#2 and C#3 in which multiple solute tracers were simultaneously injected into the Bullfrog and Prow Pass intervals, respectively, shown in Fig. 2.

2. Methods

2.1. Tracer testing objectives and strategy

The objectives of tracer testing in the fractured tuffs at the C-wells site included

- testing/validating the applicability of a dual-porosity conceptual transport model in the saturated, fractured volcanic tuffs that underlie Yucca Mountain,
- obtaining estimates of key transport parameters in the flow system, and
- assessing the applicability of laboratory-derived tracer transport parameters to field-scale transport predictions.

The latter objective is important because radionuclides cannot be tested in the field, so favorable comparisons of laboratory- and field-scale transport of nonradioactive tracers can lend credibility to the practice of using laboratory-derived radionuclide transport parameters in field-scale predictive simulations.

To accomplish all of the test objectives in a reasonable time, cross-hole, forced-gradient tracer tests were conducted in which three different tracers having different physical and chemical properties were simultaneously injected into the lower Bullfrog and Prow Pass flow systems. The test interpretations were then based on *comparing* the responses of the different tracers. The tracers used in each test included two nonsorbing solutes having different diffusion coefficients (bromide and pentafluorobenzoate) and a weakly sorbing, ion-exchanging solute (lithium ion). The properties of these solute tracers are summarized in Table 1 along with the injection masses and concentrations used in the tracer tests. Carboxylate-modified latex polystyrene microspheres were also injected in both tests to serve as colloidal tracers; the microsphere responses and their interpretations will be the subject of a future paper.

Table 1
Tracer characteristics, injection masses, and injection concentrations in the two multiple tracer tests

Tracer	PFBA	Bromide	Lithium
D_f, cm^2/s[a]	7.2×10^{-6}[b]	2.1×10^{-5}[c]	1.0×10^{-5}[c]
Sorption	none[d]	none[d]	weak (ion exchange)
Bullfrog test injection mass, kg	12.1	165.6	14.34
Bullfrog test injection concentration, mg/l[e]	1000	13,800	1200
Prow Pass test injection mass, kg	12.0	30.6	16.0[f]
Prow Pass test injection concentration, mg/l[g]	2000	5100	2670

[a] D_f = free water diffusion coefficient. Callahan et al. (2000) found that diffusion coefficients in rock matrices had the same ratio as free water diffusion coefficients for PFBA and bromide.

[b] Benson and Bowman (1994, 1996).

[c] Newman (1973)—based on ionic conductances at infinite dilution.

[d] Negligible sorption of PFBA and bromide was verified in bacth sorption tests using crushed C-wells core and water from well J-13 located about 2 km from the C-wells.

[e] Tracers were dissolved in ~ 12,000 l of groundwater.

[f] Lithium was injected as 33.3 kg LiBr and 80.8 kg LiCl.

[g] Tracers were dissolved in ~ 12,000 l of groundwater.

Several investigators have used multiple nonsorbing tracers with different diffusion coefficients in fractured rock tracer experiments as a way of distinguishing between the effects of diffusion and hydrodynamic dispersion in tracer responses (Moench, 1995; Sanford et al., 1996; Jardine et al., 1999; Maloszewski et al., 1999; Reimus and Haga, 1999; Becker and Shapiro, 2000; Callahan et al., 2000). Differences in the responses of nonsorbing tracers (with the more diffusive tracer having a lower peak normalized concentration and longer tail) have been taken as an indication of matrix diffusion; and conversely, similar or identical nonsorbing tracer responses have suggested negligible matrix diffusion. However, even when there is a significant difference in nonsorbing tracer responses, it is not possible to distinguish between true diffusion into the matrix and diffusion into stagnant (or near-stagnant) free water in the fracture system. Distinguishing between these two cases is very important for Yucca Mountain performance assessments because diffusion into the matrix implies that there will be much more stagnant water accessible to radionuclides (and hence longer travel times and lower concentrations) than if diffusion is only into free water. Diffusion into the matrix also implies that there will be much more surface area available for radionuclide sorption.

Fig. 3 shows hypothetical solute tracer responses for a cross-hole tracer test with a short injection pulse in both a single-porosity system (left-hand plot) and a dual-porosity system (right-hand plot). Separation of the nonsorbing tracer responses occurs only in the dual-porosity system. The sorbing tracer is attenuated in both time and concentration in the single-porosity system, but in the dual-porosity system, it will be attenuated very little in time if sorption occurs only in the matrix. Furthermore, if diffusion is only into stagnant free water, and not into the matrix, the peak concentration of the sorbing tracer will be higher than that of any nonsorbing tracer with a larger free diffusion coefficient (e.g., bromide compared to lithium ion). Significant time attenuation of a sorbing tracer will occur in a dual-porosity system only if matrix sorption is very strong or if significant sorption occurs in the fractures (due to fracture coating minerals or fracture fill material).

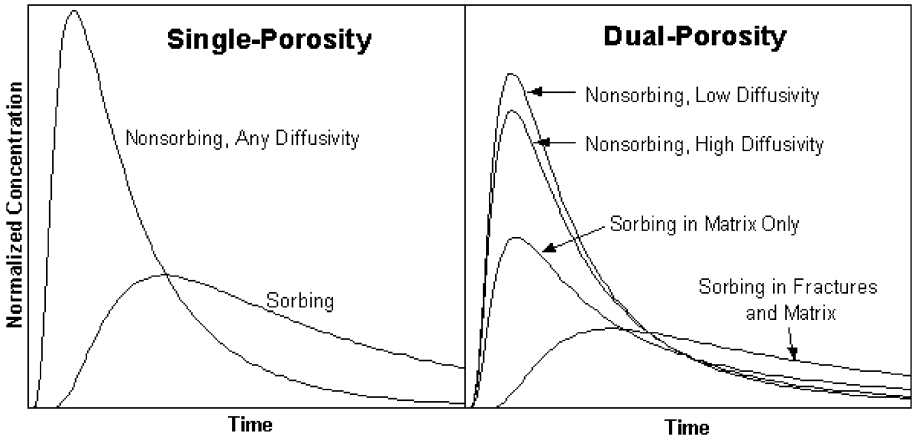

Fig. 3. Hypothetical cross-hole responses of nonsorbing and sorbing solute tracers in single-porosity and dual-porosity media. Responses were calculated using the RELAP model.

The hypothetical responses in Fig. 3 suggest that a multiple tracer test involving the simultaneous injection of nonsorbing tracers with different diffusion coefficients and a weakly sorbing tracer should allow optimal discrimination between a single-porosity system and a dual-porosity system.

2.2. Test details

The cross-hole tracer tests were conducted between wells C#2 and C#3, which are separated by about 30 m at the surface (Fig. 1). C#2 was used as the tracer injection well and C#3 as the production well in the lower Bullfrog Tuff. In the Prow Pass Tuff, C#3 was the injection well, and C#2 was the production well. The natural gradient at the C-wells site, though quite flat, is believed to be oriented in the direction from C#3 to C#2 (Fig. 1), so tracer movement in the Bullfrog test was against the gradient, and in the Prow Pass test, it was with the gradient. Prior to injecting tracers, a weak-dipole flow field was established in each test by re-injecting a fraction of the water pumped from the production well into the injection well. The production and re-injection flow rates are summarized in Table 2. Pressure transducers continuously monitored pressures between the packers, above the upper packer, and below the lower packer in each well during the tests. Because of the large differences in transmissivity of the two test intervals, the water level drawdown in the Prow Pass interval (62 m) was over an order of magnitude greater than in the Bullfrog interval (5 m) despite the fact that the production rate in the Bullfrog test was ~ 30 times greater than in the Prow Pass test.

After establishing a reasonably steady weak-dipole flow field, as indicated by stable pressures in the packed-off intervals, the recirculation of produced water into the injection well was replaced by the injection of a groundwater solution containing the three tracers. To avoid pressure or flow transients, transitions between recirculation and tracer injection were accomplished with no flow disruption. Recirculation of produced water was discontinued after 40 days in the Bullfrog test, but it was maintained throughout the Prow Pass test. The Bullfrog and Prow Pass tests were conducted for 337 and 127 days, respectively.

Water samples were collected at the production well throughout both tests using an auto-sampler, and they were manually collected from the injection interval in the Prow

Table 2
Average production and recirculation rates during the Bullfrog and Prow Pass tracer tests, and summary of flow interruptions during the Prow Pass test

Test	Production rate, l/min	Recirculation rate, l/min	Recirculation ratio
Bullfrog	568	19 (zero after 40 days)	0.033
Prow Pass	19	5.7	0.3
Interruption	**Flow shut off**	**Flow turned on**	**Duration (h)**
Prow Pass test flow interruptions			
1	11/14/98, ~ 9:00 am	11/14/98, ~ 11:00 pm	~ 14
2	11/23/98, ~ 9:00 am	11/30/98, ~ 4:00 pm	~ 175
3	12/21/98, ~ 9:00 am	1/4/99, ~ 11:00 pm	~ 337

Pass test 40 days after tracer injection. Samples were analyzed for bromide (Br^-) by liquid chromatography (conductivity detector), for pentafluorobenzoate (PFBA) by high-pressure liquid chromatography (UV absorbance detector), and for lithium (Li^+) by inductively coupled plasma-atomic emission spectroscopy (ICP-AES) at Los Alamos. Sampling of the Prow Pass injection interval confirmed that less than 0.1% of the tracer mass remained in the interval 40 days after tracer injection.

3. Results and analyses

3.1. Test results

Fig. 4 shows the normalized concentrations of the three solute tracers at the production well as a function of time during the Bullfrog test. All concentrations are normalized to the injection masses of tracers (μg/l kg injected or $\times 10^9$ l^{-1}). The axes in Fig. 4 have logarithmic scales so that the details of the breakthrough curves can be seen throughout the entire test. The fractional recoveries of the tracers were 0.69 for both bromide and PFBA, and 0.39 for lithium.

The most striking feature of the tracer breakthrough curves Fig. 4 is their bimodal shape. We believe that the double-peak responses were the result of at least two distinct fracture flow pathways between the injection and production wells that were located at

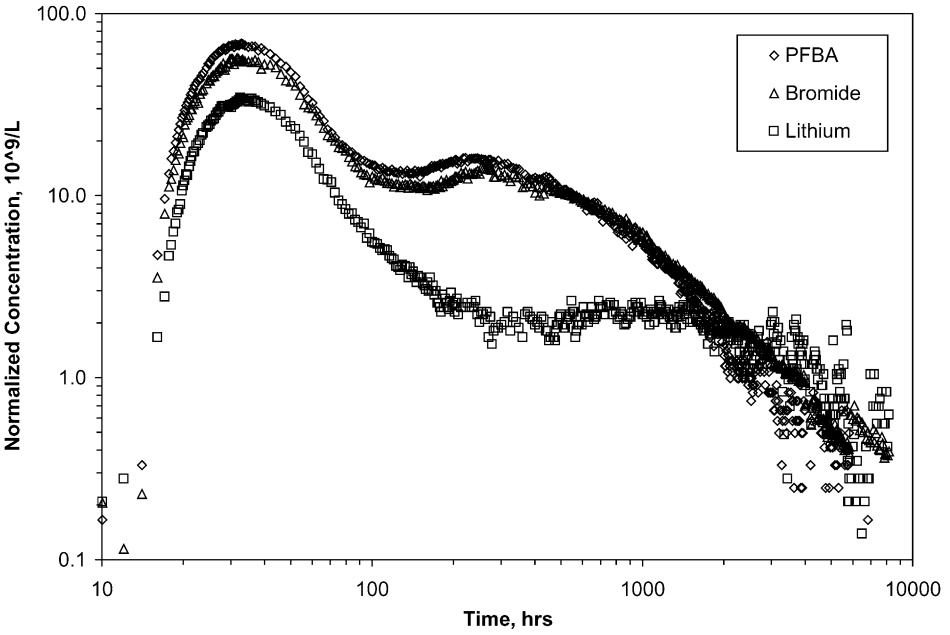

Fig. 4. Normalized tracer concentrations vs. time in the Bullfrog Tuff tracer test conducted from October 1996 to September 1997. Note the log scales of both axes.

different depths within the relatively long (~ 100 m) test interval. The flow survey information in Fig. 2 suggests that there were probably two principal zones of outflow during tracer injection into C#2 (see the triangles indicating percentages of flow during open-hole pumping). Because of the lack of mixing in the injection interval, the tracer solutions, which were injected directly below the top packer and were ~ 2% denser than the groundwater, probably sank rapidly to the bottom of the interval. Under these conditions, the majority of the tracer mass would be expected to exit C#2 from the lower flow zone, and indeed, the majority of the tracer mass (~ 60%) was associated with the second tracer peak. The first peak was apparently the result of a small percentage (~ 12%) of the tracer mass exiting C#2 from the upper flow zone. This zone was apparently more conductive (as suggested by the greater percentage of flow during open-hole pumping) and much better connected hydraulically to C#3 than the lower zone, as the travel time between the wells in this zone was much shorter. Additional evidence to support this hypothesis is obtained by comparing the PFBA response of Fig. 4 with the response of the same tracer injected into C#2 6 months prior to the start of the multiple tracer test. Fig. 5 shows that the PFBA breakthrough curve in the earlier test was a more conventional single-peak response with a peak arrival time that coincided with the arrival time of the second peak in the latter test. The earlier test was conducted in the same interval and at the same flow rates as the multiple tracer test; however, the PFBA was injected in only ~ 1000 l of tracer solution, while in the second test, it was injected in ~ 12,000 l of solution. Given that the volume of the injection interval was ~ 4300 l, it

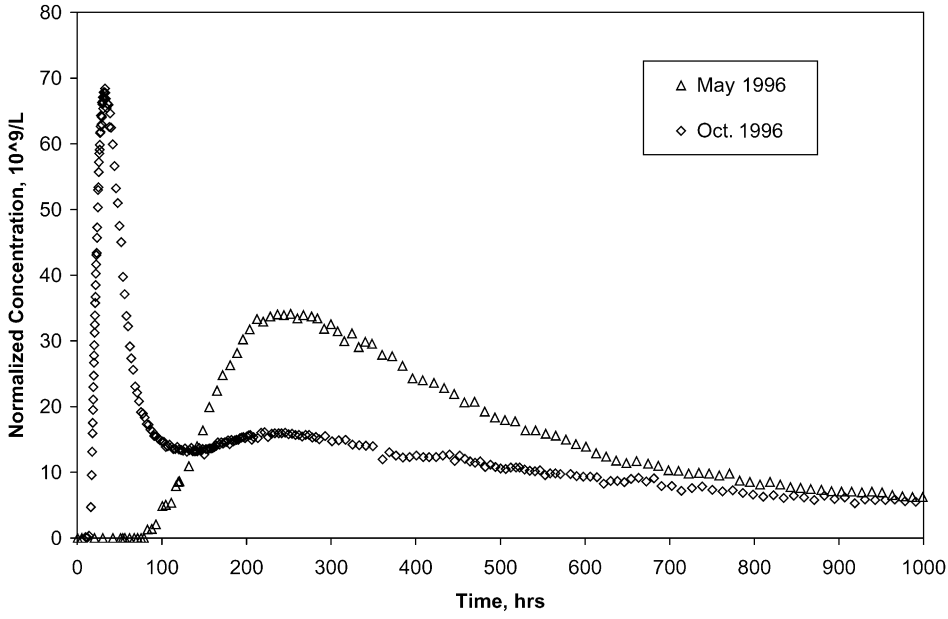

Fig. 5. Comparison of normalized PFBA responses in the Bullfrog Tuff resulting from tracer injections in May 1996 and October 1996. The test conditions were the same in both tests, but the injection solution volume was ~ 1000 l in May and ~ 12,000 l in the October.

seems logical that the ~ 1000 l of tracer solution injected in the first test would have sunk rapidly and exited the borehole via only the lower flow zone. In contrast, the ~ 12,000 l of tracer solution injected in the second test (approximately 3 interval volumes) eventually "filled up" the interval, and a fraction of the tracer mass apparently accessed the upper flow zone. PFBA concentrations in the earlier test were monitored for just over 3000 h with a total recovery of ~ 73%; at 3000 h into the second test, the PFBA recovery was ~ 58%. The lower recovery at the same time in the second test, and the fact that the shapes of the common peaks in the two tests are different, suggest that a considerable fraction of the mass injected in the latter test followed additional pathways that were not accessed in the first test.

Fig. 6 shows the normalized concentrations of the three solute tracers at the production well as a function of time during the Prow Pass test. Note that the axes in Fig. 6 have a linear scale as opposed to the logarithmic scale used in Fig. 4 for the Bullfrog test.

The Prow Pass test featured three different flow interruptions (two intentional) during the tailing portion of the test. The times and durations of these interruptions are summarized in Table 2. The first interruption was unplanned and occurred as a result of a diesel generator failure. The latter two interruptions were planned to obtain independent confirmation of matrix diffusion in the flow system. If a flow interruption is introduced during the tailing portion of a tracer test in a dual-porosity medium when tracers are diffusing back out of the matrix, then an increase in tracer concentrations should result

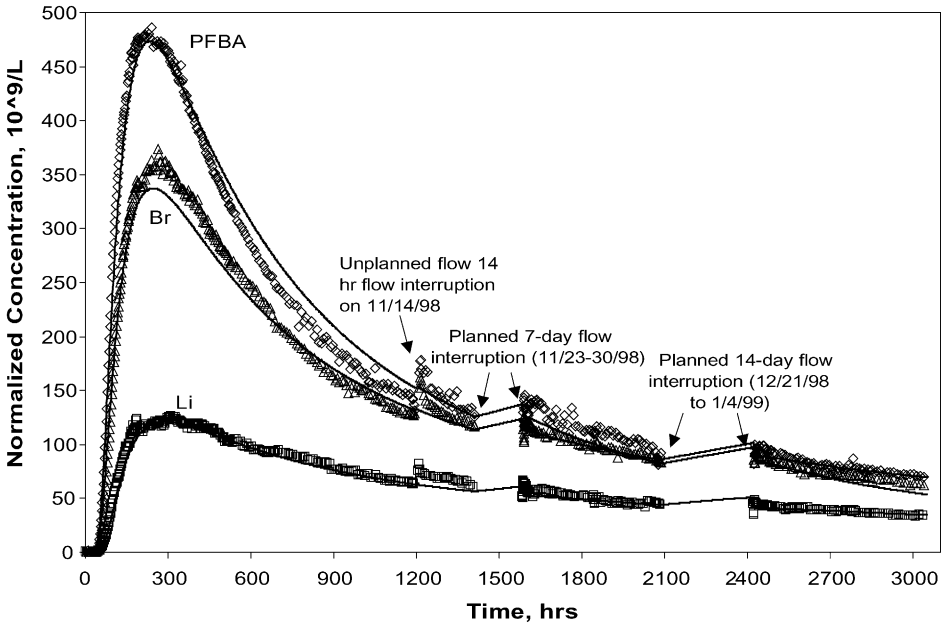

Fig. 6. Normalized tracer concentrations vs. time in the Prow Pass tracer test conducted from September 1998 to January 1999. Also shown are the RELAP/MULTRAN fits to the tracer responses. The best-fitting model parameters are provided in Table 5.

when flow is resumed (Brusseau et al., 1997; Callahan et al., 2000). Fig. 6 shows that there was indeed an increase in the tracer concentrations upon resumption of flow after each of the three interruptions. The increase after the first flow interruption was larger than the other two probably because the pump direction was initially reversed (i.e., pumping *into* the borehole). The pump had to be stopped and restarted several times, which caused significant hydraulic perturbations that may have caused some *flow* of tracers into and out of the matrix (rather than strictly diffusion). It is also possible that drift of the tracer plume during the flow interruptions could have contributed to the increases in tracer concentrations after resuming pumping, as the natural gradient flow direction was from the injection well toward the production well.

3.2. Interpretive modeling approach

To obtain estimates of transport parameters in the flow system, the semi-analytical dual-porosity transport model RELAP (REactive transport LAPlace transform inversion computer code) was used to simultaneously fit the tracer responses (Reimus and Haga, 1999). RELAP essentially combines the Laplace-domain dual-porosity transport equations derived by Maloszewski and Zuber (1984, 1985) (modified to account for linear sorption) with Laplace-domain transfer functions that describe a finite pulse injection, wellbore mixing, and recirculation. Similar approaches have been used by others (Moench, 1989, 1995; Becker and Charbeneau, 2000).

RELAP provides a simultaneous least-squares fit to up to four tracer data sets by automatically adjusting the following model parameters (which arise from the dimensionless forms of the governing equations):

- the mean fluid residence time in fractures (τ),
- the Peclet number ($Pe = W/\alpha$, where W = distance between wells, m, and α = dispersivity in fractures, m),
- the mass fraction of tracers participating in the test (f),
- a matrix diffusion mass-transfer coefficient, $\frac{\phi}{b}\sqrt{D_m}$,
- the fracture retardation factor, R_f, and
- the matrix retardation factor, R_m.

In addition, the spacing between fractures, L, can be manually adjusted to refine fits to the tails of tracer responses once a good fit to the early portion of the responses is obtained. The fractional mass participation is used as an adjustable parameter because low mass recoveries are frequently observed in field tracer tests in fractured rock (e.g., Reimus and Haga, 1999), presumably due to (1) dense tracer solutions "sinking" out of the zone of influence of pumping, (2) a significant volumetric flow of tracer solution into the matrix within the injection zone—this tracer mass will not make it to the production well during the tracer test because of very low flow velocities in the matrix, or (3) the loss of tracer mass due to stagnation points induced either by recirculation or by the superposition of the induced flow field on the ambient flow field. Although these phenomena can affect absolute tracer responses, they should not, in principle, affect the relative responses of different tracers that are injected simultaneously.

The interpretation of the tracer responses in each test involved first fitting the two nonsorbing tracer responses by simultaneously adjusting all of the parameters listed above with the constraint that the matrix diffusion coefficient, D_m, for bromide was three times that of PFBA (and therefore the matrix diffusion mass transfer coefficient, $\frac{\phi}{b}\sqrt{D_m}$, was ~ 1.7 times that of PFBA). This factor-of-three difference is based on literature data (Newman, 1973; Benson and Bowman, 1994, 1996) and the experimental diffusion cell results of Reimus et al. (1999) and Callahan et al. (2000), which are listed in Table 3. Also, R_f and R_m were held equal to 1 for the two nonsorbing tracers. This fitting procedure is justified because the tracers were injected simultaneously and should thus have experienced exactly the same flow system.

For the Bullfrog test, the two sets of tracer peaks were fitted sequentially, with the second peak being fitted after accounting for the contribution of the tail from the first peak. The model parameters were allowed to vary independently for each peak, as the peaks were assumed to represent different flow pathways with different transport characteristics. Although the tracer injection duration in the Bullfrog test was about 10 h, it was assumed that for the first peak there was a delay of 4 h followed by a 6-h injection of tracer into the pathways that resulted in the first peak. The rationale for this assumption was that there was no early peak in the May 1996 PFBA test (Fig. 5), which involved an injection of less than 1 h, so it seemed logical to assume that the earliest injected tracer solution did not follow the earliest-arriving pathways. We chose a 4-hr delay time because the injected tracer solution volume exceeded the injection interval volume at this time, and we felt that this was a reasonable criterion for when at least a portion of the tracer solution should have begun moving through the early-arriving pathways.

In contrast to the Bullfrog test, the fitting procedure for the Prow Pass test was very straightforward, as only one set of tracer peaks was observed. However, because RELAP is based on a semi-analytical Laplace transform inversion method, it was not capable of simulating the flow interruptions during the latter part of the test. To simulate these transients, the MULTRAN (multicomponent transport) code was used. MULTRAN is an implicit alternating-direction, two-dimensional finite-difference code that accounts for cation exchange, charge balance, and multicomponent diffusion in a dual-porosity transport system (Sullivan et al., 2003, this issue). The best-fitting transport parameters

Table 3
Matrix diffusion coefficients of bromide and PFBA in C-wells tuffs measured in diffusion cell experiments

Tuff lithology	Porosity	Permeability, mDarcy	L, cm[a]	Matrix diffusion coefficient, $\times 10^6$ cm^2/s		
				Br	PFBA	Br/PFBA
Central Bullfrog	0.094	0.00107	1.16	0.45	0.13	3.46
Lower Bullfrog	0.298	0.0949	0.84	1.0	0.35	2.86
Upper Prow Pass	0.272	4.72	0.91	6.0	1.9	3.16
Central Prow Pass	0.138	0.000786	1.23	0.4	0.13	3.08
Lower Prow Pass-1[b]	0.288	0.455	2.27	3.0	1.1	2.73
Lower Prow Pass-2[b]	0.288	0.455	1.82	3.0	1.0	3.0

Measured tuff porosities and permeabilities are also reported. Data taken from Reimus et al. (1999) and Callahan et al. (2000).

[a] L = thickness of tuff wafer used in diffusion cell.

[b] Diffusion coefficients were measured through two different wafers of Lower Prow Pass tuff.

obtained from RELAP fits to the tracer data up until the flow interruptions were used in MULTRAN to extend the simulations to the end of the test.

Once best simultaneous fits to the nonsorbing tracer responses in both tests were obtained, the lithium responses associated with each distinct tracer peak were fitted with RELAP by adjusting R_f and R_m while holding all other parameters equal to the values that provided the best fits to the nonsorbing tracers. However, D_m for lithium was assumed to be half that of bromide (and $\sim$ 1.5 times that of PFBA) based on ionic conductances at infinite dilution (Newman, 1973). Rate-limited sorption was not considered in the field tests because the response times were all quite long relative to typical rates of ion exchange.

RELAP provided a good match to the lithium response associated with the second peak in the Bullfrog test and also to the lithium response in the Prow Pass test. However, in the case of the first peak in the Bullfrog test, RELAP consistently overestimated the normalized concentrations in the lithium tail when the leading edge of the lithium response was fitted. The inability to fit the response of lithium ion using a linear equilibrium sorption model (K_d model) had been previously encountered when trying to fit lithium responses from laboratory-scale fracture transport experiments (Callahan et al., 2002) and also crushed rock column experiments (Sullivan et al., 2003, this issue). In these studies, it was observed that lithium transported more conservatively than K_d models predicted because the lithium injection concentration was high relative to the ionic strength of the groundwater (that is, the total cation equivalents in the system were dominated by lithium). Under these conditions, some of the lithium eluted with the anion tracers to maintain local charge balance in the system. However, when lithium injection concentrations were sufficiently dilute, local charge balance could be maintained by exchanging cations, and a K_d model more closely approximated the observed transport behavior. In the Bullfrog test, the injection concentration of lithium was $\sim$ 0.1 M, whereas the ionic strength of the C-wells groundwater was $\sim$ 0.003 M. Thus, MULTRAN was employed to match the lithium data in the first peak of the Bullfrog test using the mean residence time, Peclet number, and matrix diffusion mass transfer coefficient obtained from the best RELAP fit to the conservative tracer data and allowing the lithium ion-exchange parameters to be varied. Lithium was assumed to exchange with sodium and calcium ions based on the results of cation exchange capacity experiments conducted using C-wells tuffs (Anghel et al., 2002).

It should be noted that the relatively low tracer concentrations observed at the production well during the first peak in the Bullfrog test do not necessarily reflect the concentrations that existed in the fractures in which transport occurred; it is very likely that a significant amount of dilution occurred in the production well. For the second peak of the Bullfrog test and for the Prow Pass test, concentrations in the fractures apparently were dilute enough during the much longer residence times associated with these responses that lithium transport could be reasonably well approximated by a K_d model.

3.3. Test interpretations

The best RELAP/MULTRAN fits to the tracer breakthrough curves in the Bullfrog test are shown in Fig. 7. The RELAP fits were obtained assuming a constant production rate of 568 l/min and a constant recirculation rate of 19 l/min (3.3% of production), despite the fact

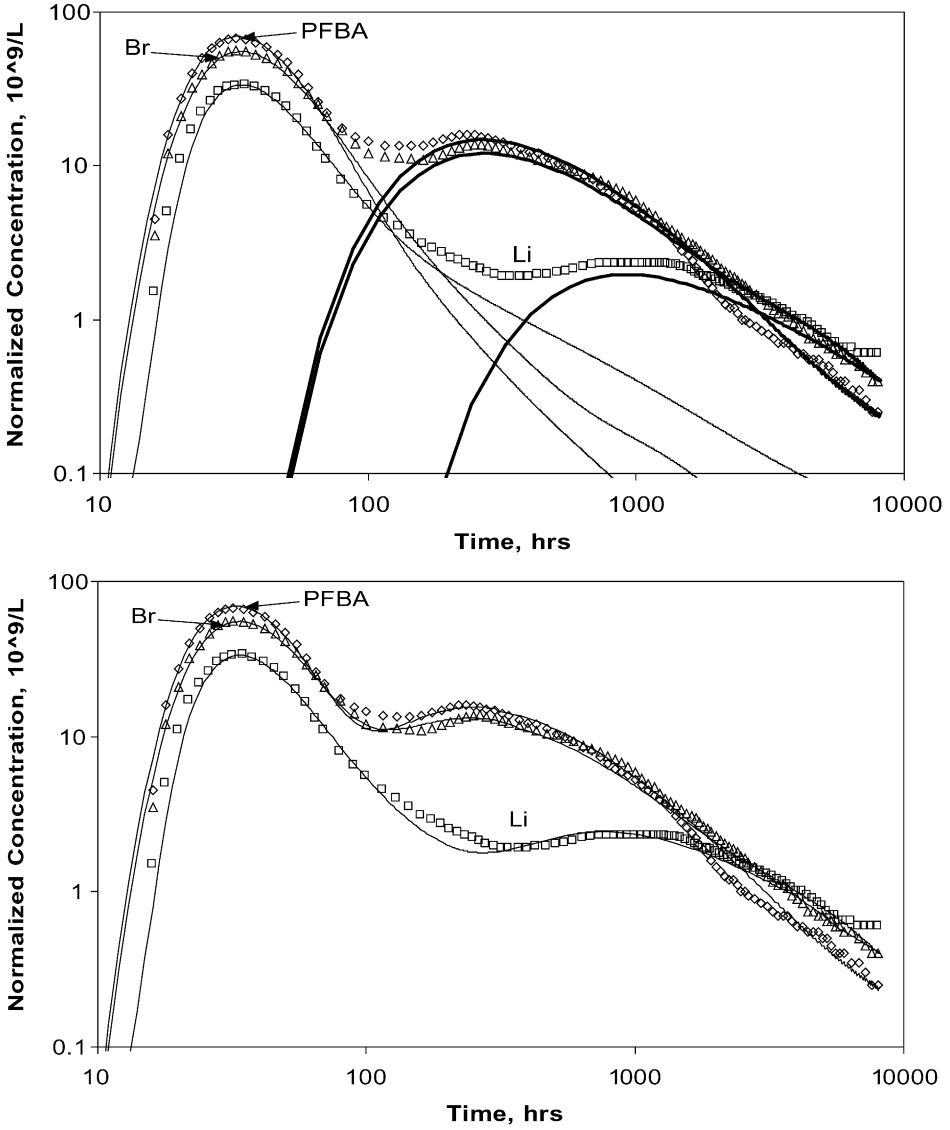

Fig. 7. RELAP and MULTRAN fits to the tracer response curves in the Bullfrog Tuff tracer test. Upper plot shows individual fits to first and second (bold lines) tracer peaks (MULTRAN and RELAP, respectively), and lower plot shows composite fits. For clarity, the data points shown are a subset of the actual data. The best-fitting model parameters are provided in Table 4.

that recirculation in the field test was stopped after 40 days. Separate MULTRAN simulations with and without recirculation after 40 days indicated that the assumption of continued recirculation after 40 days had negligible effect on the fits or the values of the fitted model parameters.

Table 4
RELAP model parameters providing the best fits to the Bullfrog tracer test data (pathway 1 and pathway 2 are associated with the first and second tracer peaks, respectively)

Parameter	Pathway 1	Pathway 2
f, mass fraction	0.115	0.60
τ, linear flow, h	36	1020
Pe, linear flow	6.5	1.6
τ, radial flow, h	30	630
Pe, radial flow	9.3	2.8
$\frac{\phi}{b}\sqrt{D_m}$ for bromide, $s^{-1/2a}$	0.0015	0.000469
Fracture spacing, cm	∞ (2.4)[b]	4.4
Lithium fracture retardation factor	1	3
Lithium matrix retardation factor	7.5[c]	33

The fits are shown in Fig. 7 (MULTRAN was used to fit first lithium peak in Fig. 7).

[a] $\frac{\phi}{b}\sqrt{D_m}$ for PFBA is 0.577 times that for bromide.

[b] Number in parentheses is the minimum fracture spacing that yields the same results as an infinite fracture spacing.

[c] Lithium response associated with first tracer peak was poorly fitted by RELAP, so MULTRAN was used to obtain a better fit, which is shown in Fig. 7.

The best-fitting model parameters from RELAP for the Bullfrog test are listed in Table 4. Note that separate estimates of τ and Pe are provided depending on whether linear flow (constant flow velocity between injection and production well) or radial flow (flow velocity inversely proportional to distance from production well) is assumed in the test interval. RELAP provides estimates for these parameters under either assumption (the quality of the fits and the other model parameters are not affected). In a heterogeneous, confined aquifer, the flow velocity to a single production well with no recirculation into an injection well is expected to vary between linear and radial (National Research Council, 1996). Thus, if it is assumed that the test interval was reasonably confined, presenting the two values of τ and *Pe* in Table 4 is a rough way of bounding these model parameter

Table 5
RELAP model parameters providing the best fits to the first 1200 h of Prow Pass tracer test data

Parameter	Parameter value
f, mass fraction	0.72
τ, linear flow, h	1210
Pe, linear flow	1.3[a]
τ, radial flow, h	610
Pe, radial flow	4.8[a]
$\frac{\phi}{b}\sqrt{D_m}$ for bromide, $s^{-1/2b}$	0.00095
Fracture spacing, cm	∞ (6.4)[c]
Lithium fracture retardation factor	1
Lithium matrix retardation factor	11.5

The fits (extended by MULTRAN simulations) are shown in Fig. 6.

[a] The Peclet numbers were adjusted to correct for the theoretical dispersion caused by the partial recirculation flow field (see text). Peclet numbers obtained directly from RELAP were 0.9 (linear flow) and 1.9 (radial flow).

[b] $\frac{\phi}{b}\sqrt{D_m}$ for PFBA is 0.577 times that for bromide.

[c] Number in parentheses is the minimum fracture spacing that yields the same results as an infinite fracture spacing.

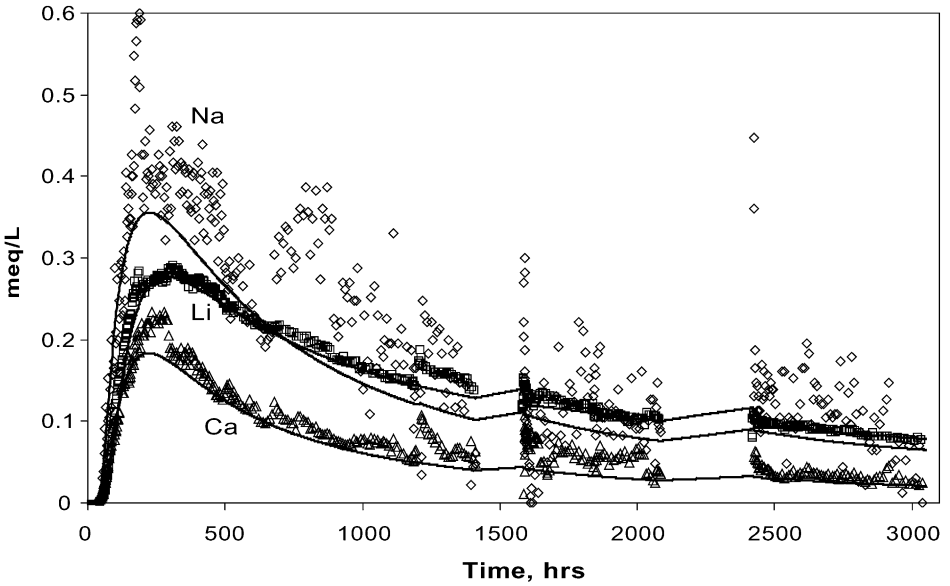

Fig. 8. MULTRAN fits to cation responses (background subtracted) in the Prow Pass tracer test. Scatter for sodium is due to the fact that background is large relative to signal.

estimates as a result of flow field uncertainty. Although the Bullfrog flow system was not perfectly confined, this approach should still yield reasonable bounds for τ and *Pe*, as the flow velocities in pathways carrying tracers from C#2 to C#3 should have started out relatively high due to the recirculation into C#2, gone through a minimum, and then increased again in the vicinity of C#3. Thus, the weak dipole should have resulted in a flow pattern that was intermediate between linear and radial flow.

The best RELAP/MULTRAN fits to the Prow Pass tracer test data are shown in Fig. 6, and Table 5 gives the best-fitting RELAP model parameters (obtained by simulating the first 1200 h of the test, prior to the first flow interruption). MULTRAN was used after the first flow interruption to model the remainder of the test using the best-fitting parameters from RELAP to extend the simulations. Because the tracer concentrations were significantly higher in this test than in the Bullfrog test, it was possible to determine the responses of the cations (sodium and calcium) that exchanged with lithium during the test. Fig. 8 shows the responses of lithium, sodium, and calcium ions in the Prow Pass test, expressed as meq/l vs. time. MULTRAN fits to the data are also included in Fig. 8. Although not shown here, it was confirmed that the total cation and anion charges balanced each other, as they must, throughout the test.

4. Discussion and conclusions

Even without quantitative parameter estimation, it is clear that the tracer responses in both the Bullfrog and Prow Pass tests (Figs. 4 and 6) are consistent with a dual-porosity

conceptual transport model for the fractured volcanic tuffs (Fig. 3). It is simply not possible to account for the differences in the bromide and PFBA responses, or the relatively small time attenuation but significant concentration attenuation of the lithium response relative to the nonsorbing tracers (in the Prow Pass test and the first peak of the Bullfrog test) without invoking diffusion between flowing fractures and stagnant matrix water. Although some diffusion into stagnant free water within the fracture system cannot be ruled out, it is unlikely that there would be as much concentration attenuation of lithium relative to the nonsorbing solutes if there was not a significant amount of surface area available for sorption (i.e., in the matrix).

Estimates of transport parameters that can be used directly in solute transport models were derived from the best-fitting model parameters in Tables 4 and 5. These parameter estimates are presented in Table 6 as ranges of values that are consistent with the tracer test interpretation(s). Additional discussion of these ranges and how they were derived is provided in the following sections.

4.1. Matrix diffusion mass transfer

The quantitative estimates of the lumped mass transfer parameter $\frac{\phi}{b}\sqrt{D_m}$ for bromide in Tables 4 and 5 are based on the assumption that bromide has a diffusion coefficient that is a factor of 3 greater than PFBA (Table 3; also, Reimus et al., 1999; Callahan et al., 2000). It is worth noting that RELAP simulations in which a finite matrix was assumed (i.e., a finite spacing between fractures) offered a slightly better fit to the tracer responses associated with the second peak of the Bullfrog test than simulations assuming an infinite matrix. This result suggests that tracer molecules may have diffused far enough into the matrix to begin encountering molecules from neighboring fractures. Alternatively, the tracers may have encountered impermeable boundaries at a finite distance into the matrix that impeded further diffusion. For the first peak in the Bullfrog test and for the Prow Pass test, a finite matrix offered no improvement to tracer data fits than an infinite matrix. In

Table 6
Transport parameter estimates deduced from the Bullfrog and Prow Pass tracer tests (provided as ranges of values—see text for explanations)

Parameter	Prow Pass		Bullfrog	
	Lower bound	Upper bound	Lower bound	Upper bound
Effective flow porosity	0.003	0.006	0.003[a]	0.034[a]
Longitudinal dispersivity, m[b]	6.3	61.5	3.2	62.5
$\frac{\phi}{b}\sqrt{D_m}$ for radionuclides, $s^{1/2}$[c]	0.00054	0.00095	0.00027	0.0015
Fracture aperture, cm	0.18	1.06	0.085	1.28
Fracture spacing, cm	6.4	∞	2.4	∞
Ratio of stagnant to flowing water volumes	1.8–10.2	∞	0.3–15.2	∞

[a] These estimates assume that 75% of the production flow was associated with flow pathways that resulted in the first tracer peak and 25% was associated with the second tracer peak (based on flow survey information).

[b] Lower bounds assume Peclet numbers for radial flow and 30 m travel distance; upper bounds assume Peclet numbers for linear flow and interval thicknesses as travel distances.

[c] Assumes that bromide and PFBA effectively bound sizes and diffusion coefficients of radionuclide solution species.

these cases, it can only be stated that the fracture spacing must have exceeded some threshold value below which the tracer responses would be affected. The applicable threshold values for the first Bullfrog test peak and for the Prow Pass test were estimated by adjusting the fracture spacing in RELAP until the simulated tracer responses began to differ significantly from the infinite matrix responses. These results are presented in Tables 4–6 as lower bounds for fracture spacing.

4.2. Fracture apertures

An estimate of the average fracture aperture ($2b$) experienced by the tracers in the Bullfrog and Prow Pass tests can be obtained from the estimate of the lumped diffusive mass transfer parameter, $\frac{\phi}{b}\sqrt{D_m}$, provided independent estimates of matrix porosity, ϕ, and matrix diffusion coefficients, D_m, are available. Using estimates of ϕ determined from laboratory measurements and D_m for bromide and PFBA from diffusion cell tests (Table 3), estimates of $2b$ range from 0.085 to 1.28 cm in the Bullfrog Tuff and from 0.18 to 1.06 cm in the Prow Pass Tuff, as listed in Table 6. Because the long tracer test intervals in each test both included more than one major lithology (Fig. 2), it was necessary to estimate $2b$ for each major lithologic unit in each interval. The fact that there is a positive correlation between matrix porosity and matrix diffusion coefficient results in a relatively large range of aperture estimates. If it is assumed that the flow pathways associated with the first tracer peak in the Bullfrog test were in the central Bullfrog unit and the pathways associated with the second tracer peak were in the lower Bullfrog unit, then the aperture estimates in these two units correspond to the two extremes listed in Table 6. These aperture estimates based on tracer responses should be distinguished from friction loss or cubic law aperture estimates that are obtained from hydraulic responses (Tsang, 1992).

4.3. Ratios of stagnant water to flowing water volumes

Estimates of the ratio of stagnant water volume to flowing water volume in the flow system(s) can be calculated from estimates of fracture spacings, matrix porosities, and fracture apertures discussed in the previous two sections (ratio $= \phi L/2b - b$). Ranges of these estimates are listed in Table 6. The ranges are rather large because the estimates of fracture aperture and fracture spacing have large ranges. The upper bound ratios for both tracer tests are listed as infinite because all tracer responses could be fitted reasonably well assuming infinite fracture spacing. The ranges listed as lower bounds in Table 6 were obtained from the combinations of fracture apertures and fracture spacings that resulted in the highest and lowest ratios (excluding infinite). These ratios plus 1 can be considered physical retardation factors for nonsorbing species in the flow system when flow rates are low enough that there is ample time for solutes to diffuse throughout the stagnant water in the system (Robinson, 1994).

4.4. Lithium sorption behavior

Tables 4 and 5 list the best-fitting values of the lithium fracture and matrix retardation factors (R_f and R_m, respectively) for the Bullfrog and Prow Pass tests. Note that the R_f

values are 1 for both the Prow Pass test and for the first peak in the Bullfrog test, implying negligible retardation within the fractures and sorption only in the matrix. However, a fracture retardation factor of 1 does not necessarily imply that sorption did not occur on fracture surfaces; it merely suggests that the majority of the lithium sorption occurred *after* diffusion to sorptive surfaces. For the second peak in the Bullfrog test, the lithium response was best fitted with $R_f = 3$ and $R_m = 33$, implying some sorption in fractures and a large amount of sorption in the matrix.

Matrix K_d values were deduced from the fitted matrix retardation factors by simple rearrangement of the expression defining the retardation factor:

$$K_d = \frac{\phi}{\rho_B}(R_m - 1) \quad (1)$$

Because the K_d values depend on the matrix porosity, values are listed in Table 7 for each lithologic unit in which transport may have occurred during each test (matrix porosities from Table 3 were used). The R_m value associated with the first lithium peak in the Bullfrog test (Table 4) was obtained by fitting the rising limb of the lithium response using RELAP. However, because it was necessary to use MULTRAN to achieve a reasonable fit to the tail of the response, the K_d value for this peak was estimated from the ion-exchange parameters that yielded the best fit to the lithium data (see Sullivan et al., 2003, this issue) rather than from the R_m value obtained from RELAP. The best-fitting ion exchange parameters suggested a highly nonlinear sorption isotherm for lithium in the matrix, so K_d

Table 7
Lithium partition coefficients (K_d values) derived from the field tracer tests assuming transport in different lithologies within the test intervals, and corresponding laboratory measurements of K_d values in these intervals

Parameter	Field K_d	Laboratory K_d[a]
Prow Pass matrix K_d assuming Central Prow Pass Tuff	0.66	0.13 (0.26 at infinite dilution)
Prow Pass matrix K_d assuming Lower Prow Pass Tuff	1.65	0.084 (0.44 at infinite dilution)
Bullfrog matrix K_d in Pathway 1 assuming Central Bullfrog Tuff[b]	0.13–12.6 (nonlinear)[c]	0.19 (0.44 at infinite dilution)
Bullfrog matrix K_d in Pathway 1 assuming Lower Bullfrog Tuff[b]	0.50–48.8 (nonlinear)[c]	0.32 (1.64 at infinite dilution)
Bullfrog matrix K_d in Pathway 2 assuming Central Bullfrog Tuff[b]	1.36	0.19 (0.44 at infinite dilution)
Bullfrog matrix K_d in Pathway 2 assuming Lower Bullfrog Tuff[b]	5.27	0.32 (1.64 at infinite dilution)

Laboratory K_d values taken from Anghel et al. (2002).

[a] Values at "infinite dilution" obtained from slopes of Langmuir isotherm fits to the data (asymptotic slope at very low concentrations; i.e., $K_L S_{max}$). Other values obtained from a simple linear fit to the entire range of data.

[b] "Pathway 1" refers to pathways that resulted in the first tracer peak in the Bullfrog reactive tracer test, and "Pathway 2" refers to pathways that resulted in the second peak in this test. K_d values were calculated from the *smallest* matrix retardation factors obtained from alternative interpretations of the test.

[c] First number corresponds to K_d value calculated at 100 mg/l Li^+ using the three-component cation exchange model parameters yielding the best fit to the first lithium peak (see Sullivan et al., this issue); the second number corresponds to K_d value calculated at 1 mg/l Li^+ concentration using same model parameters.

values are reported in Table 7 for lithium concentrations of both 100 mg/l (low K_d value) and 1 mg/l (high K_d value). This range of concentrations should reasonably bound the concentrations experienced in the field test.

Laboratory batch measurements of lithium sorption onto crushed tuff from C-wells cores were previously conducted (Anghel et al., 2002). The range of laboratory-derived K_d values associated with each unit that could have participated in the Bullfrog and Prow Pass tests is listed in Table 7 next to each corresponding field-derived K_d value.

The lithium K_d values deduced from the field tracer tests (for any given lithologic unit) are consistently higher than the corresponding K_d values measured in the laboratory. The only exception is that the field K_d value may have been somewhat lower than the laboratory K_d value in the flow pathways resulting in the first peak in the Bullfrog test. In general, these results suggest that the use of laboratory-derived K_d values to predict sorbing species transport in fractured tuffs near the C-wells would tend to underpredict sorption. The fact that the field K_d values tended to be greater than the laboratory K_d values suggests that lithium may have come in contact with alteration minerals in the field that were absent or depleted in the lab samples.

4.5. Effective flow porosity

Contaminant transport predictions are generally very sensitive to assumed flow porosities because transport rates are directly proportional to specific discharge divided by flow porosity. The effective flow porosity in a cross-hole tracer test without recirculation can be estimated from the following equation, which assumes a confined, homogeneous, isotropic flow system:

$$\phi = \frac{Q\tau}{\pi W^2 T} \tag{2}$$

where ϕ = flow porosity, Q = production flow rate, m^3/h, and, T = formation thickness (assumed to be interval length).

With recirculation, the situation is complicated by the fact that there is a hypothetical stagnation point, and hence, the mean tracer residence time theoretically approaches infinity. However, the interpretive method described in this paper allows for incomplete tracer mass recoveries that could result from stagnation, so a finite and unbiased estimate of the mean tracer residence time can always be obtained.

Table 6 gives the effective flow porosities calculated using Eq. (2) for the Bullfrog and Prow Pass tests. The upper and lower bounds given in Table 6 were calculated using the mean tracer residence times obtained assuming linear and radial flow, respectively (values in Tables 4 and 5). Also, in the Bullfrog test, it was assumed that 75% of the total production flow rate was associated with the first tracer peak and 25% was associated with the second tracer peak (based on flow survey information suggesting that more flow occurred in the upper part of the injection interval in C#2—see Fig. 2).

The flow porosities in Table 6 intuitively seem high given what is known about the fracture system at the C-wells. The large estimates obtained from Eq. (2) could be due to heterogeneities in the flow field. Flow is undoubtedly not radial, as assumed in Eq. (2), but

rather, it very likely follows tortuous pathways between the injection and production wells. Such tortuous pathways seem especially likely at the C-wells because fracturing was predominantly perpendicular to the tracer transport direction with predominantly high-angle dips. Furthermore, it is conceivable that a single high-conductivity feature such as a large, open fracture or fault could transmit the vast majority of the flow to the production well. If this feature does not pass near the injection well, the effective flow rate drawing tracers to the production well could be greatly reduced relative to what would occur in a radial flow field.

4.6. Longitudinal dispersivity

Longitudinal dispersivity estimates from cross-hole tracer tests generally have considerable uncertainty due to (1) uncertainty in the actual tracer transport distance (the actual flow pathways followed by tracers), (2) whether the flow field is radial, linear, or some combination, (3) the amount of apparent dispersion caused by a poorly mixed injection wellbore or density/buoyancy effects, and (4) the amount of apparent dispersion caused by recirculation or the superimposed ambient flow field. It is beyond the scope of this paper to address in detail the possible effects of each of these uncertainties on the longitudinal dispersivity estimates provided in Table 6. However, these estimates are in reasonably good agreement with dispersivities derived from field tests of similar length scales (Neuman, 1990; Gelhar et al., 1992). The estimates in Table 6 can be considered "upper and lower bounds" that were obtained as follows:

(1) The maximum transport distance was assumed to be the distance from the top of one packed-off interval to the bottom of the other (80–100 m), while the minimum transport distance was assumed to be the linear distance between the wells ($\sim$ 30 m),

(2) The radial and linear Peclet numbers were both used to obtain estimates of the dispersivity ($\alpha = W/Pe$), and the most extreme values were used for the upper and lower bounds,

(3) Dispersion caused by recirculation in the Prow Pass test was "subtracted out" by

(3.1) obtaining a simulated tracer response for a tracer test with 30% recirculation in a homogeneous, isotropic medium using a particle-tracking code (Reimus, 1996),
(3.2) calculating the variance of the particle residence times in (3.1),
(3.3) calculating the variance of the tracer response in the actual field test from $\sigma^2 = 2(\tau^2/Pe)$ (Reimus et al., 1999), where σ^2 is the variance,
(3.4) subtracting the variance in (3.2) from the variance in (3.3) to obtain the variance due to "true hydrodynamic dispersion" in the flow system (this assumes that the variance due to recirculation and the variance due to true dispersion are independent), and
(3.5) rearranging the expression in (3.3) to obtain the Peclet number, and hence dispersivity, that represents true hydrodynamic dispersion, i.e., $\sigma^2 = 2(\tau^2/Pe)$.

Corrections for dispersion caused by recirculation in the Bullfrog test were negligible. No attempt was made to account for density/buoyancy effects or the effects of the ambient flow field on the longitudinal dispersivity estimates.

4.7. Concluding remarks

The authors recognize that the tracer test interpretations using primarily a semi-analytical solution method that assumes an idealized geometry and steady flow rates is a considerable simplification of reality. Numerical models could certainly be used to account for greater system heterogeneity. Also, more sophisticated semi-analytical representations of dual-porosity systems, such as the multi-rate diffusion model of Haggerty and Gorelick (1995), could be applied. However, the information available to support these more sophisticated representations of the flow and transport system is sparse to nonexistent. Furthermore, we consider the agreement between the relatively simple semi-analytical model (RELAP) and the tracer responses to be very good (Fig. 6 and 7). Although the introduction of additional model complexity could do nothing but improve this agreement, it appears that all of the critical features of the tracer responses have been effectively captured, and the introduction of additional complexity, especially in light of the minimal information to support it, is not justified.

One must also keep in mind that the tracer test results are intended to support predictive calculations that span much larger time and distance scales than represented by the tests. With this in mind, we set out to capture the important transport processes with as concise a model as possible, so that others could incorporate a relatively simple model on a local scale into a more sophisticated flow model that captures the important hydraulic features of the larger-scale flow system. We believe that the C-wells tracer tests and their interpretations presented in this paper accomplished this objective.

Acknowledgements

We gratefully acknowledge the support provided by M. J. Umari, J. Gemmell, J. Darnell, and J. Earle of the U.S. Geological Survey at the C-wells site. A. Humphrey, A. Noell, and S. Thornton of Los Alamos also provided a great deal of field support. The manuscript benefited from the constructive reviews of P. Hsieh and an anonymous reviewer. This work was supported by the Yucca Mountain Site Characterization Project Office as part of the Civilian Radioactive Waste Management Program. This Project is managed by the U.S. Department of Energy, Yucca Mountain Site Characterization Project.

References

Anghel, I., Turin, H.J., Reimus, P.W., 2002. Lithium sorption to Yucca Mountain Tuffs. Applied Geochemistry 17, 819–824.

Becker, M.W., Charbeneau, R.J., 2000. First-passage-time transfer functions for groundwater tracer tests conducted in radially convergent flow. J. Contam. Hydrol. 40, 299–310.

Becker, M.W., Shapiro, A.M., 2000. Tracer transport in fractured crystalline rock: evidence of non-diffusive breakthrough tailing. Water Resour. Res. 36 (7), 1677–1686.

Benson, C.F., Bowman, R.S., 1994. Tri- and tetrafluorobenzoates as nonreactive tracers in soil and groundwater. Soil Sci. Soc. Am. J. 58 (4), 1123–1129.

Benson, C.F., Bowman, R.S., 1996. Erratum: tri- and tetrafluorobenzoates as nonreactive tracers in soil and groundwater. Soil Sci. Soc. Am. J. 60 (6), 1780.

Brusseau, M.L., Hu, Q., Srivastava, R., 1997. Using flow interruption to identify factors causing nonideal contaminant transport. J. Contam. Hydrol. 24, 205–219.

Callahan, T.J., Reimus, P.W., Bowman, R.S., Haga, M.J., 2000. Using multiple experimental methods to determine fracture/matrix interactions and dispersion of nonreactive solutes in saturated volcanic tuff. Water Resour. Res. 36 (12), 3547–3558.

Callahan, T.J., Reimus, P.W., Lichtner, P.C., Bowman, R.S., 2002. Multicomponent effects on the transport of cations undergoing ion exchange in fractured media. Proceedings of the International Groundwater Symposium, "Bridging the Gap Between Measurement and Modeling in Heterogeneous Media," Intl. Assoc. of Hydraul. Res., Lawrence Berkeley National Laboratory, Berkeley, CA, 25–28 March.

Callahan, T.J., Reimus, P.W., Lichtner, P.C., Bowman, R.S., submitted for publication. Multicomponent effects on the transport of cations undergoing ion exchange in fractured media. IAHR International Groundwater Symposium Proceedings, Berkeley, CA.

Eddebbarh, A.A., Zyvoloski, G.A., Robinson, B.A., Kwicklis, E.M., Reimus, P.W., Arnold, B.W., Corbet, T., Kuzio, S.P., Faunt, C., 2003. The saturated zone at Yucca Mountain: an overview of the characterization and assessment of the saturated zone as a barrier to potential radionuclide migration. J. Contam. Hydrol. 62–63C, 477–493 (this issue).

Geldon, A.L., 1993. Preliminary hydrogeologic assessment of boreholes UE-25c#1, UE-25c#2, and UE-25c#3, Yucca Mountain, Nye County, NV, 1993. USGS/WRI-92-4016, Denver, CO.

Geldon, A.L., 1996. Results and interpretation of preliminary aquifer tests in boreholes UE-25c#1, UE-25c#2, and UE-25c#3, Yucca Mountain, Nye County, NV. USGS/WRI-94-W-0412, Denver, CO.

Gelhar, L.W., Welty, C., Rehfeldt, K.R., 1992. A critical review of data on field-scale dispersion in aquifers. Water Resour. Res. 28 (7), 1955–1974.

Grisak, G.E., Pickens, J.F., 1980. Solute transport through fractured media: 1. The effect of matrix diffusion. Water Resour. Res. 16, 719–730.

Haggerty, R., Gorelick, S.M., 1995. Multiple-rate mass transfer for modeling diffusion and surface reactions in media with pore-scale heterogeneity. Water Resour. Res. 31 (10), 2383–2400.

Jardine, P.M., Sanford, W.E., Gwo, J.P., Reedy, O.C., Hicks, D.S., Riggs, J.S., Bailey, W.B., 1999. Quantifying diffusive mass transfer in fractured shale bedrock. Water Resour. Res. 35 (7), 2015–2030.

Maloszewski, P., Zuber, A., 1984. Interpretation of artificial and environmental tracers in fissured rocks with a porous matrix. Isotope Hydrology. International Atomic Energy Agency (IAEA), Vienna, Austria, pp. 635–651.

Maloszewski, P., Zuber, A., 1985. On the theory of tracer experiments in fissured rocks with a porous matrix. J. Hydrol. 79, 333–358.

Maloszewski, P., Herrmann, A., Zuber, A., 1999. Interpretation of tracer tests performed in a fractured rock of the Lange Bramke Basin, Germany. Hydrogeol. J. 7, 209–218.

Moench, A.F., 1989. Convergent radial dispersion: a Laplace transform solution for aquifer tracer testing. Water Resour. Res. 25 (3), 439–447.

Moench, A.F., 1995. Convergent radial dispersion in a double-porosity aquifer with fracture skin: analytical solution and application to a field experiment in fractured chalk. Water Resour. Res. 31 (8), 1823–1835.

National Research Council, 1996. Rock Fractures and Fluid Flow: Contemporary Understanding and Applications. National Academy Press, Washington, DC, pp. 252–259.

Neretnieks, I., 1980. Diffusion in the rock matrix: an important factor in radionuclide retardation? J. Geophys. Res. 85, 4379–4397.

Neuman, S.P., 1990. Universal scaling of hydraulic conductivities and dispersivities in geologic media. Water Resour. Res. 26 (8), 1749–1758.

Newman, J.S., 1973. Electrochemical Systems. Prentice-Hall, Englewood Cliffs, NJ.

Reimus, P.W., 1996. Predictions of tracer transport in interwell tracer tests at the C-hole complex. LA-13160-MS. Los Alamos National Laboratory, Los Alamos, NM.

Reimus, P.W., Haga, M.J., 1999. Analysis of tracer responses in the BULLION forced-gradient experiment at Pahute Mesa, NV. LA-13615-MS. Los Alamos National Laboratory, Los Alamos, NM.

Reimus, P.W., Adams, A., Haga, M.J., Humphrey, A., Callahan, T., Anghel, I., Counce, D. (with contributions

from USGS staff), 1999. Results and interpretation of hydraulic and tracer testing in the Prow Pass Tuff at the C-holes. Yucca Mountain Site Characterization Project Milestone Report SP32E7M4. Los Alamos National Laboratory, Los Alamos, NM.

Robinson, B.A., 1994. A strategy for validating a conceptual model for radionuclide migration in the saturated zone beneath Yucca Mountain. Radioact. Waste Manage. Environ. Restor. 19, 73–96.

Sanford, W.E., Shropshire, R.G., Kip Solomon, D., 1996. Dissolved gas tracers in ground-water: simplified injection sampling and analysis. Water Resour. Res. 32 (6), 1635–1642.

Sullivan, E.J., Reimus, P.W., Counce, D.A., 2003. Transport of a reactive tracer in saturated alluvium described using a three-component cation-exchange model. J. Contam. Hydrol. 62–63C, 675–694 (this issue).

Tang, D.H., Frind, E.O., Sudicky, E.A., 1981. Contaminant transport in a fractured porous media: analytical solution for a single fracture. Water Resour. Res. 17 (3), 555–564.

Tsang, Y.W., 1992. Usage of "equivalent apertures" for rock fractures as derived from hydraulic and tracer tests. Water Resour. Res. 28 (5), 1451–1455.